



**Ocean Cryosphere Exchanges in Antarctica:**

**Impacts on Climate and the Earth system**

**'Fast-track' sensitivity of freshwater fluxes to climate scenarios**

Deliverable D4.1



OCEAN:ICE is co-funded by the European Union, Horizon Europe Funding Programme for research and innovation under grant agreement Nr. 101060452 and by UK Research and Innovation

<https://ocean-ice.eu/>

**About this document**

**Deliverable:** D4.1 'Fast-track' sensitivity of freshwater fluxes to climate scenarios

**Work Package:** WP4 Quantification of Antarctic Ice Sheet 'deep uncertainty' and freshwater fluxes under climate forcing

**Delivery date:** 25 April 2024

**Type of document:** Report

**Dissemination level:** Public

**Lead beneficiary and author:** PP7-Université Libre de Bruxelles (ULB): Frank Pattyn

**Contributors (Researchers involved in the deliverable):**

PP7 - Université Libre de Bruxelles (ULB): Violaine COULON, Frank PATTYN

PP 14 - University of Northumbria at Newcastle (UNN): Jan DE RYDT, Qing QIN

**Review:**

PP1: Danish Meteorological Institute (DMI): Chiara Bearzotti ([chb@dmu.dk](mailto:chb@dmu.dk))

**Disclaimer:** Funded by the European Union and UK Research and Innovation. Views and opinions expressed are however those of the authors only and do not necessarily reflect those of the European Union or UK Research and Innovation. Neither the European Union nor UK Research and Innovation can be held responsible for them.

**Cover sheet:** Credits to NASA/GSFC/OIB

## History of changes

Version	Date	Description	Authors (A) & Reviewers (R)
1	25 April 2024	First version delivered to the European Commission.	As listed on the second page.
2	7 October 2024	Revision after the 1 <sup>st</sup> EC review, comments of the reviewers have been addressed: 1) List of references has been added. 2) Captions to the figures 1, 2 and 4 have been slightly integrated. Figure 4 has been enlarged. 3) We added a supplementary Table S1 that lists the parameters that are shown in Fig. 2. Delivery to the European Commission.	A: Frank Pattyn (ULB) R: C. Bearzotti (DMI)
3	15 October 2024	The statements on the confidentiality have been removed.	C. Bearzotti (DMI)
4	27 March 2025	In the Open Science section (2.2), the DOI of the dataset on Zenodo has been added.	C. Bearzotti (DMI)

## Table of contents

1. Publishable summary .....	5
2. Work performed and main achievements .....	6
2.1 Description of the work performed.....	6
2.2 Open Science .....	9
3. Results .....	10
4. References .....	17
5. Impact.....	20
Annex 1: Supplement Table S1: Parameters governing glaciological processes.....	21

## 1. Publishable summary

As global temperatures rise, Antarctica's grounded ice sheet and floating ice shelves are losing mass at an accelerating rate, releasing meltwater into the Southern Ocean. This increasing freshwater discharge poses significant implications for global climate dynamics. We now have clear evidence that freshwater discharges from Antarctica (ice-shelf melting, iceberg calving, subglacial discharge and surface runoff) are impacting the oceanography of the surrounding oceans, underscoring the urgent need to integrate these effects into climate models. In previous CMIP rounds, models either assumed that the ice sheets were in mass balance, or that discharge from the ice sheets was constant in time. Consequently, climate projections lack a detailed representation of spatiotemporal trends in ice-sheet freshwater fluxes and their impact on the global climate system, introducing unquantified uncertainties in future climate and sea-level projections. In this deliverable, we present a dataset that offers projections of freshwater fluxes from the Antarctic ice sheet and uncertainty estimates spanning from the present-day to the year 2300 that can be implemented as a forcing for climate models that do not include interactive ice sheets. These projections are derived from an ensemble of historically calibrated standalone ice sheet model projections generated with the Kori-ULB ice flow model (<https://github.com/FrankPat/Kori-ULB>), under different climate scenarios up to 2300. We assess the sensitivity and spread in freshwater fluxes projections in response to climate forcing and a comprehensive range of uncertain glaciological processes.

## 2. Work performed and main achievements

### 2.1 Description of the work performed

ULB has produced with the standalone ice-sheet model Kori-ULB ([Pattyn et al., 2017](#); [Coulon et al., 2024](#); [Kazmierczak et al., 2024](#), <https://github.com/FrankPat/Kori-ULB>) an ensemble of historically-calibrated pan-Antarctic simulations between 1990 and 2300, forced by atmospheric and oceanic projections inferred from a subset of models from the sixth phase of the Coupled Model Intercomparison Project (CMIP6) under low- and very high-emission scenarios. They enable us to investigate the sensitivity of Antarctic freshwater fluxes to uncertain physical processes (Table 1) and climate scenarios.

To comprehensively explore a range of uncertain glaciological processes, we designed a perturbed parameter ensemble including 8 key parameters (see Table 1) that govern the ice dynamics (basal melt, calving, basal sliding, and ice-shelf damage) and the climate forcing. We use a Latin hypercube sampling to create 100 distinct parameter vectors, producing a 100-member ensemble. Ensemble design, model setup and results (section 3) were discussed with UNN in regular meetings.

The Kori-ULB model is a vertically integrated, thermomechanical, hybrid ice-sheet–ice-shelf model. The ice flow is represented as a combination of the shallow-ice (SIA) and shallow-shelf (SSA) approximations for grounded ice, while only the shallow-shelf approximation is applied for floating ice shelves ([Bueler and Brown, 2009](#); [Winkelmann et al., 2011](#)). To account for grounding-line migration, a flux condition (related to the ice thickness at the grounding line; [Schoof, 2007](#)) is imposed at the grounding line following the implementation by Pollard and DeConto ([2012a, 2020](#)). Basal sliding is introduced as a Weertman sliding law, i.e.  $v_b = -A_b |\tau_b|^{m-1} \tau_b$ , where  $\tau_b$  is the basal shear stress;  $v_b$  the basal velocity;  $A_b$  the basal sliding coefficient, whose values are inferred following the nudging method of [Pollard and DeConto \(2012b\)](#); and  $m$  a sliding exponent. Basal melting underneath the floating ice shelves is determined by different sub-shelf melt parameterisation schemes, such as the PICO model ([Reese et al., 2018](#)), the plume model ([Lazeroms et al., 2019](#)), as well as simplified parameterisations ([Jourdain et al., 2020](#); [Favier et al., 2019](#)). Similarly, calving at the ice front is determined by a crevasse depth law (depending on the combined penetration depths of surface and basal crevasses, relative to total ice thickness; [Pollard et al., 2015](#)), a Von Mises law (depending on tensile stresses and frontal velocities; [Morlighem et al., 2016](#)), and a simple minimum thickness law ([Wilner et al., 2023](#)). The calving front position is defined using the levelset method ([Bondzio et al., 2016](#)). In addition, the effect of the propagation and penetration of fractures, called damage, on the ice flow (softening the ice, accelerating its flow and potentially promoting further damage development) is accounted for in Kori-ULB by establishing a direct link between the amount of damage (often expressed as the ratio between the total crevasse depth and the local ice thickness) and ice viscosity (following [Sun et al., 2017](#)). Such parameterization can be considered as a precursor to a Marine Ice Cliff Instability (MICI), as implemented in DeConto et al. ([2016, 2021](#)). Finally, basal melting underneath the grounded ice sheet is calculated based on the difference between the basal temperature gradient (influenced by both the geothermal heat flux and frictional heating at the base) and the gradient corrected for pressure melting. All simulations are performed at spatial resolutions of 16 km and 8 km (taken as an uncertain parameter in the ensemble – see Table 1).

Our ice-sheet simulations start in 1990 to allow comparisons with observations over the satellite era ([Otosaka et al., 2023](#); [Davison et al., 2023](#)). Ice-sheet initial conditions are provided by an inverse simulation nudging towards present-day ice-sheet geometry ([Pollard and DeConto, 2012b](#); [Bernales et al., 2017](#); [Coulon et al., 2024](#)). Hindcasts of the behaviour of the AIS over the period 1990–2014 are produced using surface mass balance (SMB) and air temperature conditions for the 1995–2014 period

based on the Regional Atmospheric Climate Model (RACMO2.3p2; [van Wessem et al., 2018](#)) and present-day ocean temperature and salinity fields of the coastal ocean around Antarctica taken from [Jourdain et al. \(2020\)](#). As of the year 2015, changes in atmospheric and oceanic properties derived from a subset of CMIP6 climate models (MRI-ESM2-0, IPSL-CM6A-LR, CESM2-WACCM, and UKESM1-0-LL) are used as forcing until the year 2300. The forcing applied is derived from both the Shared Socioeconomic Pathway (SSP) 5-8.5 and 1-2.6 scenarios to estimate the possible evolution of Antarctic freshwater fluxes to a wide range of climate forcing. Climate forcing is derived in the form of yearly averaged atmospheric (air temperature and SMB) and oceanic (temperature and salinity) anomalies compared with the 1995–2014 mean, added to reference fields used over the historical period ([van Wessem et al., 2018](#), [Jourdain et al., 2020](#)).

**Table 1:** Parameters governing glaciological processes along with their uncertainty ranges used in the uncertainty analysis.

Parameter	Uncertainty range	Units
Sub-shelf melt parameterisation ( $M_{\text{param}}$ )	PICO model ( $M_{\text{PICO}}$ ) Plume model ( $M_{\text{plume}}$ ) Local quadratic parameterisation ( $M_{\text{quad}}$ ) ISMIP6 non-local quadratic parameterisation ( $M_{\text{JD20}}$ ) ISMIP6 non-local quadratic parameterisation including a dependency on the local slope ( $M_{\text{JD20s}}$ )	-
Effective ice-ocean heat flux ( $\Gamma_{\text{eff}}$ )	$\gamma_T^*$ in $M_{\text{PICO}}$ : $0.1\text{-}10 \times 10^{-5}$ $C_d^{1/2} \Gamma_{TS}$ in $M_{\text{plume}}$ : $1\text{-}10 \times 10^{-4}$ $\gamma_T$ in $M_{\text{quad}}$ : $1\text{-}10 \times 10^{-4}$ $\gamma_0$ in $M_{\text{JD20}}$ : $1\text{-}4 \times 10^4$ $\gamma_0$ in $M_{\text{JD20s}}$ : $1\text{-}4 \times 10^6$	$\text{m s}^{-1}$ - $\text{m s}^{-1}$ $\text{m yr}^{-1}$ $\text{m yr}^{-1}$
Calving law ( $C_{\text{law}}$ )	Crevasse depth law (CD) Von mises law (VM) Minimum Thickness law (MT)	-
Calving parameter ( $C_{\text{par}}$ )	Critical crevasse ratio in CD: [0.5 - 1] Tensile stress threshold in VM: [25 - 1000] Minimum ice thickness threshold in MT : [50 - 400]	- kPa m
Exponent in sliding law (m)	[1 - 5]	-
Maximum damage ratio (dam)	[0 - 0.5]	-
Spatial resolution ( $\Delta x$ )	8 - 16	km
CMIP6 GCM (GCM)	MRI-ESM2-0, UKESM1-0-LL, IPSL-CM6A-LR, CESM2-WACCM	-

We then perform a Bayesian calibration of our 100-member ensemble of ice-sheet model simulations by comparing the model results over the past decades with a series of estimates of regional net mass balance from the latest Ice Sheet Mass Balance Inter-comparison Exercise (IMBIE; [Otosaka et al., 2023](#), see Table 2). This allows a higher predictive weight to be attributed to model simulations that demonstrate skill at reproducing the observations ([Ritz et al., 2015](#); [Nias et al., 2019](#); [Werneck et al., 2020](#), [Coulon et al., 2024](#)). In particular, we determine the posterior probability distribution of the uncertain input parameters starting from the prior probability distribution (assumed to follow a uniform distribution) using Bayes' theorem. For more details on the calibration procedure, we refer to



[Coulon et al., 2024](#). Note that we here estimate the structural error by multiplying the observational error by a factor of 8.

**Table 2:** Observational constraints of Antarctic regional mass balance from the Ice Sheet Mass Balance Inter-comparison Exercise (IMBIE; [Otosaka et al., 2023](#)) used for the Bayesian calibration of the ensemble.

	WAIS (Gt yr <sup>-1</sup> )	EAIS (Gt yr <sup>-1</sup> )	APIS (Gt yr <sup>-1</sup> )
<b>1992-1996</b>	-37 ± 19	-27 ± 33	-7 ± 11
<b>1997-2001</b>	-42 ± 19	21 ± 32	2 ± 11
<b>2002-2006</b>	-64 ± 20	21 ± 34	-20 ± 11
<b>2007-2016</b>	-129 ± 23	19 ± 36	-21 ± 12
<b>2012-2016</b>	-131 ± 21	-13 ± 35	-6 ± 13
<b>2017-2020</b>	-94 ± 25	0 ± 47	-21 ± 12

## 2.2 Open Science

The version of Kori-ULB used to perform the simulations is accessible on GitHub (<https://github.com/VioCoulon/Kori-ULB/tree/OceanIce>). The method applied to design and calibrate the ensemble of simulations is explained in detail in [Coulon et al. \(2024\)](#).

The fast-track dataset produced is made available:

- as NetCDF files ('SSP126\_FWF\_1990\_2300.nc' and 'SSP585\_FWF\_1990\_2300.nc') on the OCEAN:ICE ERDDAP (<https://er1.s4oceanice.eu/erddap/index.html>)
- on Zenodo: <https://zenodo.org/records/14162776>

The content of this deliverable will be presented in a Poster entitled '*Constraining projections of future freshwater fluxes from Antarctica*' in session CR2.2 – *Ice-sheet and climate interactions* at the EGU 2024 conference taking place in Vienna, Austria from 14 to 19 April 2024. The content of the deliverable and the dataset produced will also be presented to the OCEAN:ICE community at an OCEAN:ICE Annual Storyline Meeting on Deep Uncertainty in Freshwater Fluxes Led by Frank Pattyn (ULB) taking place online on the 2nd of May 2024.

The authors are also planning to publish these results in a manuscript to be published in open access.

### 3. Results

We have produced ensembles of historically-calibrated Antarctic simulations, with projections of freshwater fluxes (ice-shelf melting, iceberg calving, and surface mass balance) under low and very-high emission scenarios for 27 drainage basins until 2300. Our simulations encompass both the historical period (1990-2020) and future projections until the year 2300 under distinct climate scenarios. These Antarctic freshwater flux projections will be implemented as forcing for climate models within WP5 and WP6 (Fast track). We assume that changes in ice thickness above flotation represent net mass-balance changes. Changes in cumulative surface, sub-ice-shelf and subglacial fluxes reflect surface mass balance, sub-shelf melt and subglacial melt (underneath the grounded ice sheet) fluxes, respectively. Subtracting these three terms from the net change in thickness gives an estimate of losses due to iceberg calving. Note that since subglacial melt underneath the grounded ice sheet represents a minor component of the Antarctic ice sheet mass balance and subglacial water is not routed around, we do not provide estimates of the subglacial discharge across the grounding line here.

The behaviour of the ensemble over the historical period is displayed in Figure 1. From 1990 to 2020, calibrated net mass balance and calving and sub-shelf melt fluxes are in good agreement with satellite-based estimates ([Otosaka et al., 2023](#), [Davison et al., 2023](#), [Adusumilli et al., 2020](#)). The spread of the posterior distribution is reduced compared with the prior distribution, showing that the calibration is effective in reducing uncertainty in the model hindcasts even though a large tolerance was assigned for model structural error. The resulting posterior distributions of the parameter space are displayed in Figure 2. Rapid grounded-ice mass losses are reproduced around the margins of the ice sheet, especially in the Amundsen Sea Embayment and in Aurora Basin in East Antarctica (Fig. 1 d-e), similar to observations over the past decades ([Smith et al., 2020](#); [Rignot et al., 2019](#)).

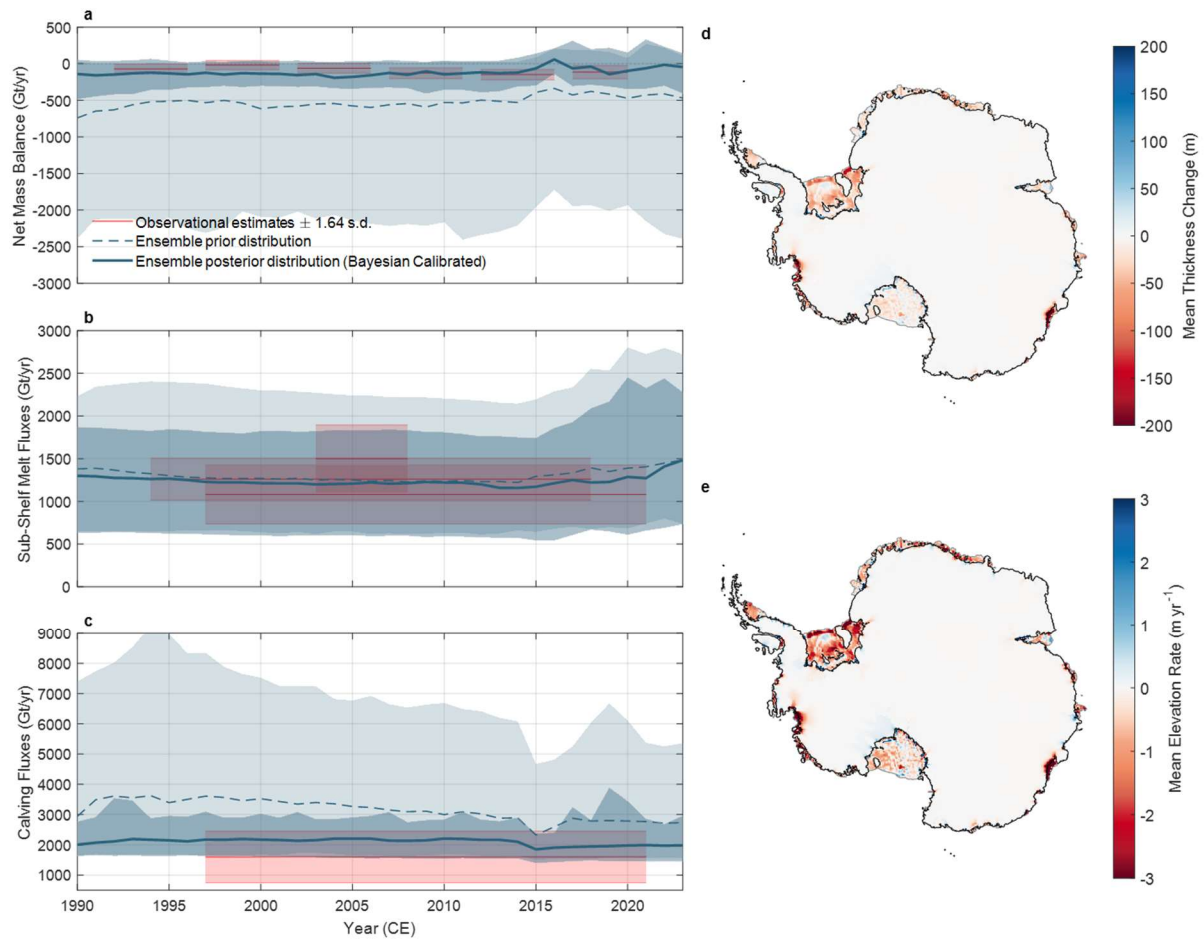


**Fig. 1:** Evolution of the 100-member ensemble of simulations of the Antarctic ice sheet over the historical period (1990-2020). Evolution of the Antarctic ice-sheet net mass balance (considering volume above flotation only), i.e. the rate of mass change contributing to sea-level rise (a); the sub-shelf melt fluxes (b); and the calving fluxes (c), over the historical period and comparison with observations (red lines and shaded areas represent the uncertainty of the observations, shown as  $\pm 1.64\sigma$ ; [Otosaka et al., 2023](#), [Davison et al., 2023](#), [Adusumilli et al., 2020](#)). Dashed lines and pale blue shaded areas represent the ensemble prior distributions (medians and 5 %–95 % probability intervals), while solid lines and dark blue shaded areas represent the posterior (Bayesian-calibrated medians and 5 %–95 % probability intervals) distributions. The spatial pattern of historical mass change over the ensemble is illustrated by the Bayesian-calibrated mean thickness change (e) and rate of elevation change (f) over the period 1990-2020. Black lines show the ensemble mean grounding-line position (allowed to evolve during the hindcast). The 100-member ensemble of simulations is produced using Latin hypercube sampling in the parameter space defined in Table 1.

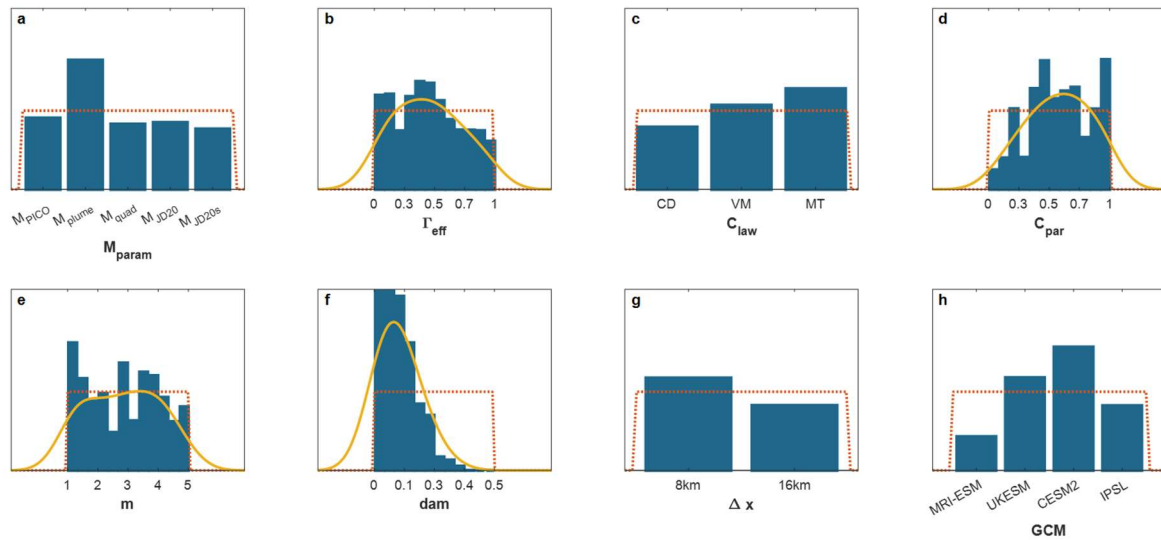


**Fig. 2:** Posterior parameter probability distributions and density histograms resulting from the calibration. Posterior parameter density histograms and probability distribution functions approximated using kernel density estimation (lines) are shown for all parameters except discretely distributed parameters. The parameters are detailed in the supplementary Table S1. The prior distributions are shown as dashed orange lines while the posterior distributions are shown as yellow lines. Weighted histograms are shown in blue.

Similarly, the differences between the prior and posterior distributions of the sea-level projections are shown in Figure 3. The spread of the posterior distribution is reduced compared with the prior TO distribution. Over the historical period, the calibrated median sea-level contribution is in line with the cumulative ice sheet mass changes from the latest IMBIE assessment ([Otosaka et al., 2023](#); Figure 3a–b). Throughout the century, mass loss primarily occurs in the Amundsen Sea Embayment and Totten Glacier area under both socio-economic pathways (Figure 4). The pattern of mass loss under both emission pathways starts to diverge after the end of the century. While mass loss remains essentially limited to the Amundsen Sea Embayment under SSP1-2.6, the very high-emission scenario (SSP5-8.5) exhibits an acceleration of mass loss in the Amundsen Sea sector, as well as the onset of grounding-line retreat in Siple Coast (Ross area) and Filchner-Ronne ice shelf area (Weddell Sea).

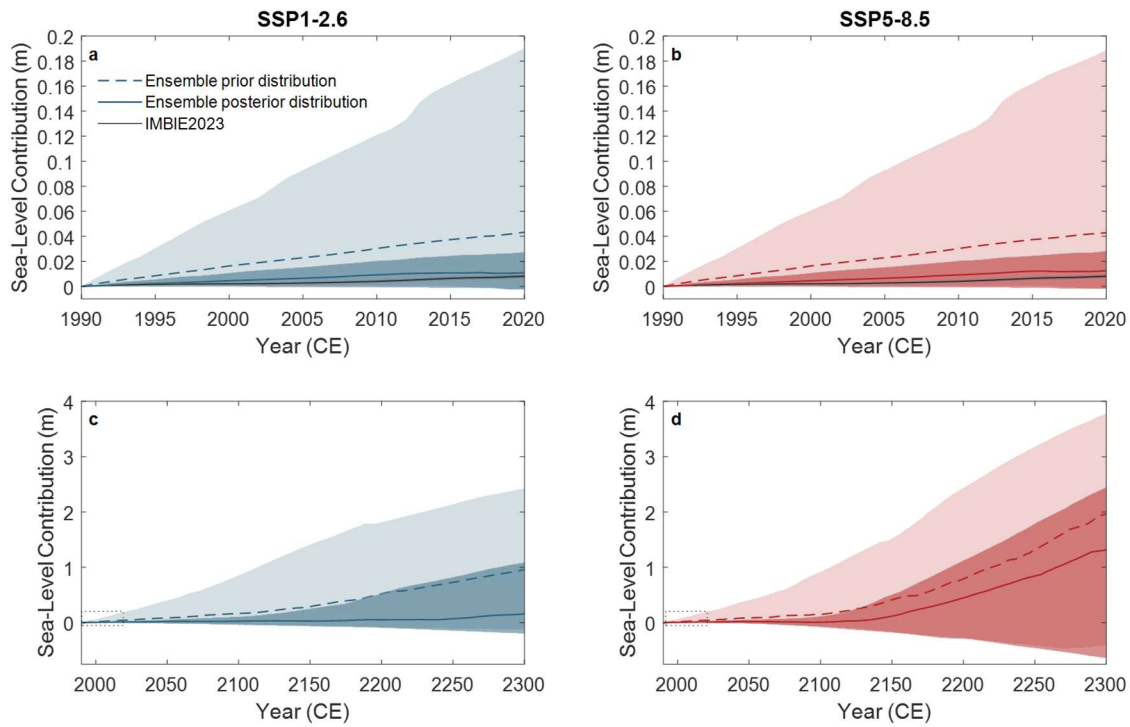


**Fig. 3:** Comparison of the prior and posterior distributions of projected Antarctic contribution to global mean sea-level rise between 1990 and 2300. Evolution of the ensemble projected contribution to sea-level from the Antarctic ice sheet until 2020 (a-b) and 2300 (c-d), under the Shared Socio-Economic Pathways (SSP) 1-2.6 and SSP5-8.5 scenarios (N=100 per SSP scenario). The ensemble uncalibrated median (dashed lines) and 5–95% probability interval (light dashed area) are compared to the Bayesian calibrated ensemble median (solid lines) and 5–95% probability interval (dark shaded area). The cumulative ice sheet mass changes from the latest IMBIE assessment ([Otosaka et al., 2023](#)) are shown in a–b for comparison.

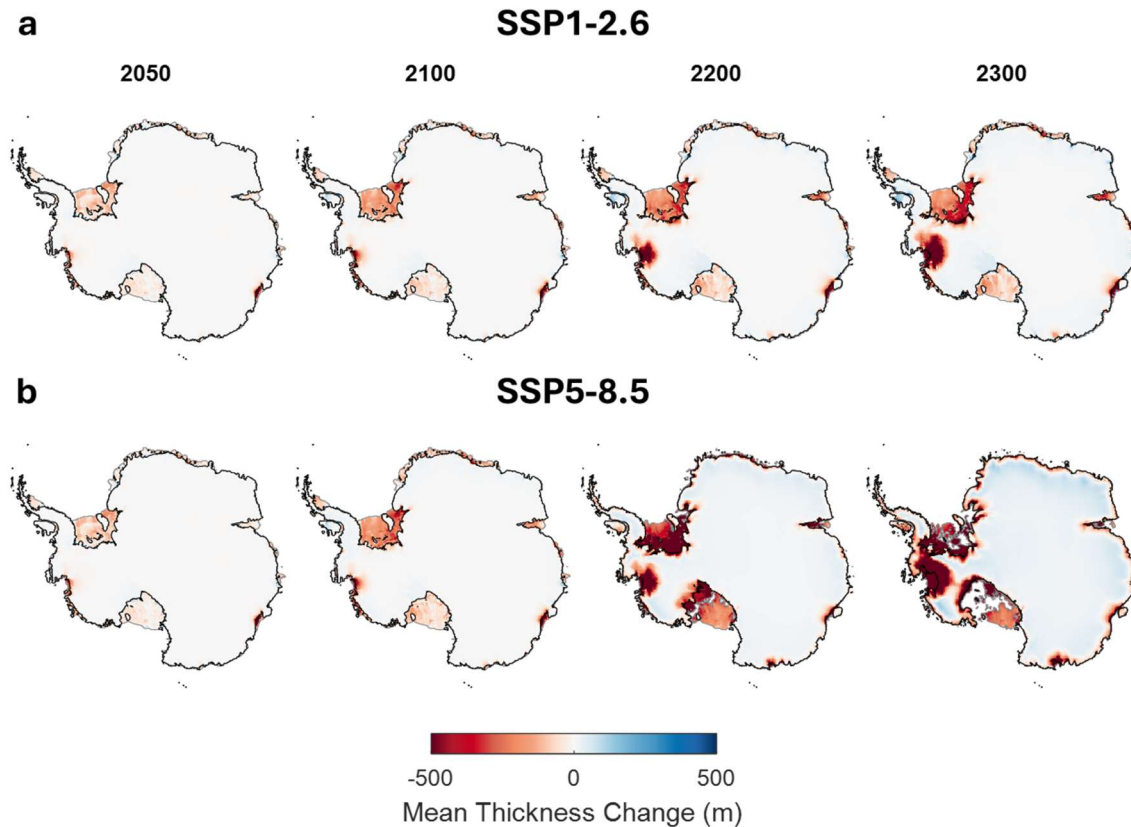


**Fig. 4:** Mean ice thickness change under the shared socioeconomic pathways (SSP) 1-2.6 (a) and 5-8.5 (b) at different points in time until 2300. For each scenario, the mean thickness change at a given point is computed using the Bayesian calibrated mean of the ensemble ( $N=100$ ). Black lines show the ensemble mean grounding line positions.

This projected Antarctic mass loss will release meltwater into the Southern Ocean, posing significant implications for global climate dynamics. The projected historically calibrated trends in the distribution of calving, ice shelf basal melt, and surface mass balance fluxes for the entire Antarctic ice sheet under the low- and very-high emission pathways are displayed in Figure 5. Overall, sub-shelf melting emerges as the dominant freshwater contributor, with an increasing influence in both climate scenarios, projected to surpass the initially dominating calving fluxes by around 2050 under both scenarios. This increase in sub-shelf melt fluxes is particularly strong in the SSP5-8.5 scenario, peaking around 2150 and then declining with the collapse of the ice shelves. In contrast, calving fluxes follow a more stable trajectory, remaining relatively constant over time. Under both emission scenarios, calving fluxes decrease in response to the increasing sub-shelf melting. Under SSP5-8.5, however, calving fluxes slightly increase again after the 2150 peak in sub-shelf melt, with this increase being particularly pronounced within the 5-95% probability interval. Furthermore, surface mass balance is projected to decrease after 2100 under SSP5-8.5 due to an increase in surface runoff with warmer air temperatures.

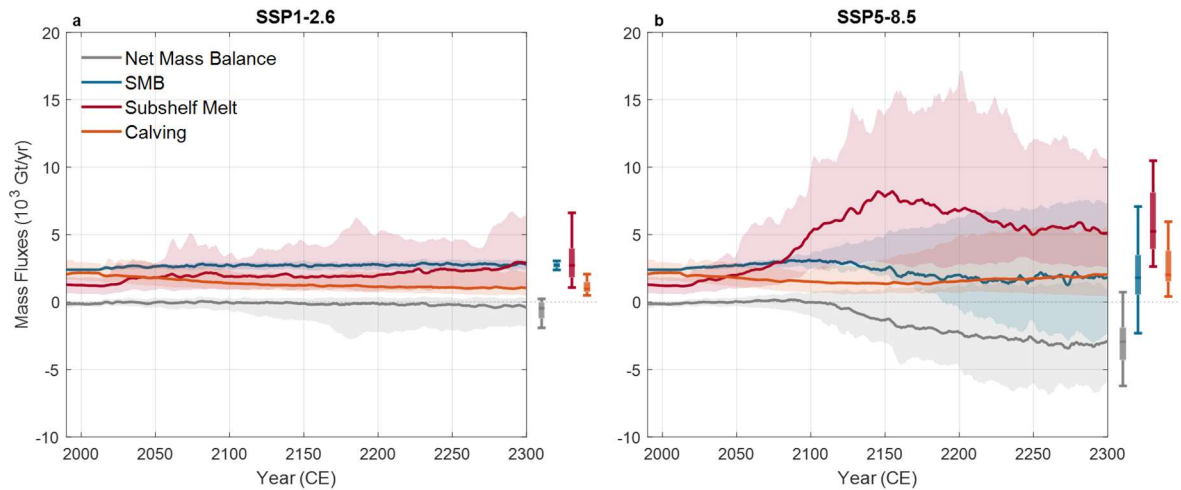


**Fig. 5:** Calibrated probabilistic projections of the Antarctic ice sheet mass balance components until 2300 under SSP1-2.6 (a) and SSP5-8.5 (b). Solid lines and shaded regions show the median and 5-95% probability intervals ( $N=100$ ), with a 5-year running average applied. Boxes and whiskers show [5;25;50;75;95] percentiles for the year 2300. Positive SMB fluxes represent mass gains while positive sub-shelf melt and calving fluxes represent mass losses. Note that the ice-sheet net mass balance does not represent the sum of all mass balance components but instead considers changes in volume above flotation and may therefore be interpreted as the rate of mass change contributing to sea-level rise.

Spatial trends in future freshwater discharge will significantly influence the oceanography of the surrounding oceans. For this reason, projected trends in calving, sub-shelf melt and surface mass balance fluxes are provided for 27 Antarctic drainage basins (Figure 6). These can be grouped in the three ocean sectors of Antarctica. The evolution of the projected freshwater fluxes in each ocean sector of Antarctica over the historical period and until the year 2300 are displayed in Figures 7 and 8, respectively.

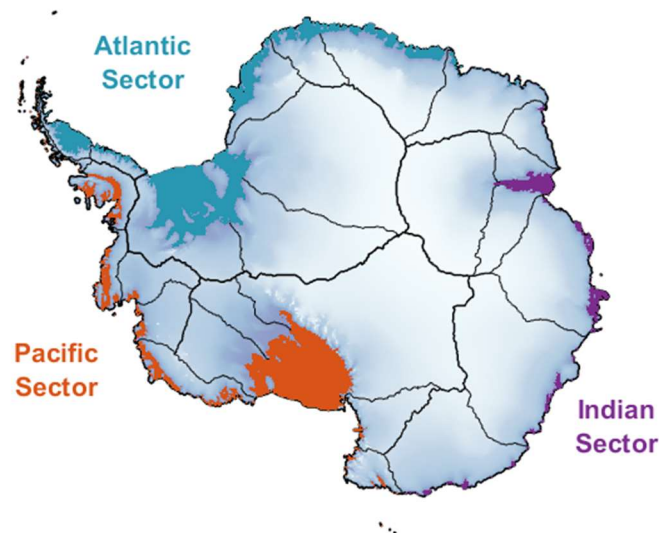


**Fig. 6:** Delineation of the 27 drainage basins and the Pacific (orange), Atlantic (blue), and Indian (purple) ocean sectors of Antarctica used for the regional analysis.



The posterior distributions of the modelled calving and sub-shelf melt fluxes are overall in line with observations (Davison et al., 2023) over the historical period (1990-2020; see Figure 7). In the Pacific sector, about 50% of the total freshwater flux comes from melting, which has increased slightly in recent years to about 650 Gt/yr. Meanwhile, calving has remained relatively stable at about 550 Gt/yr. Conversely, in the Atlantic sector, calving dominates, contributing roughly 70% of total freshwater fluxes at about 850 Gt/yr, while melt contributions hover around 300 Gt/yr. Similarly, in the Indian sector, calving is the main contributor to freshwater fluxes, accounting for about 75% of total fluxes at approximately 650 Gt/yr, alongside a small increase in melt fluxes to about 200 Gt/yr.

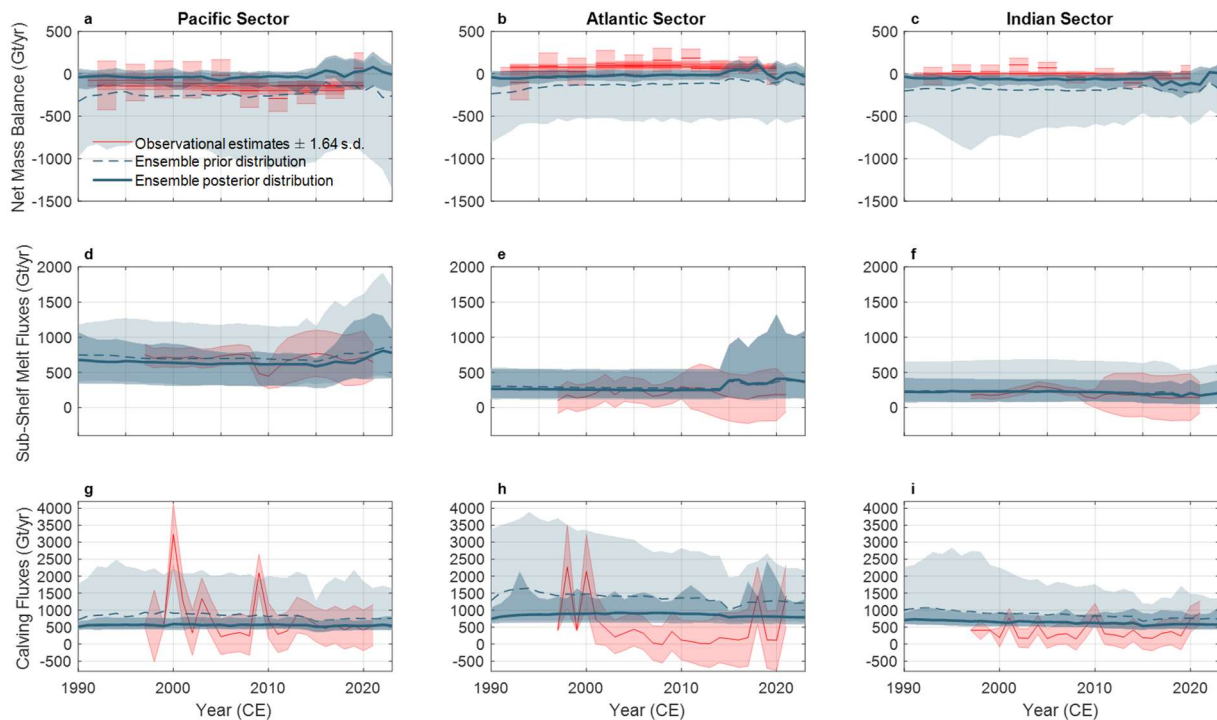


**Fig. 7:** Evolution of the regional net mass balance (considering volume above flotation only) (a); the sub-shelf melt fluxes (b); and the calving fluxes (c), over the historical period for each ocean sector of Antarctica and comparison with observations (red lines and shaded areas represent the uncertainty of the observations, shown as  $\pm 1.64\sigma$ ; Nilsson et al., 2022, Davison et al., 2023).

Looking towards future projections under different climate scenarios, notable shifts in sectoral freshwater flux dynamics are expected (Figure 8). Under the SSP1-2.6 scenario, there is a projected slight increase in snow accumulation and surface mass balance across all sectors due to limited surface melt and runoff. In addition, sub-shelf melt fluxes are projected to rise in all oceanic sectors, leading to a decrease in calving fluxes and establishing sub-shelf melt as the primary source of freshwater flux. Under SSP5-8.5, initial increases in SMB are followed by declines beyond the end of the century, particularly pronounced in the Pacific sector, as runoff fluxes increase (Kittel et al., 2021; Coulon et al., 2024). A significant increase in sub-shelf melt is also forecasted, with sub-shelf melt fluxes expected to surpass calving as the primary source of freshwater flux across all sectors by around 2050. However, a subsequent slight resurgence in calving fluxes is projected, particularly within the 5-95% probability interval, potentially reaching fluxes of the same magnitude as the sub-shelf melting.

In summary, the majority of Antarctica's projected freshwater fluxes will be discharged in the Pacific Ocean sector, closely followed by the Atlantic sector. These freshwater fluxes may become particularly significant under very-high warming scenarios (SSP5-8.5), linked to a progressive collapse of the West Antarctic ice shelves, and will be primarily discharged locally through sub-shelf melting.



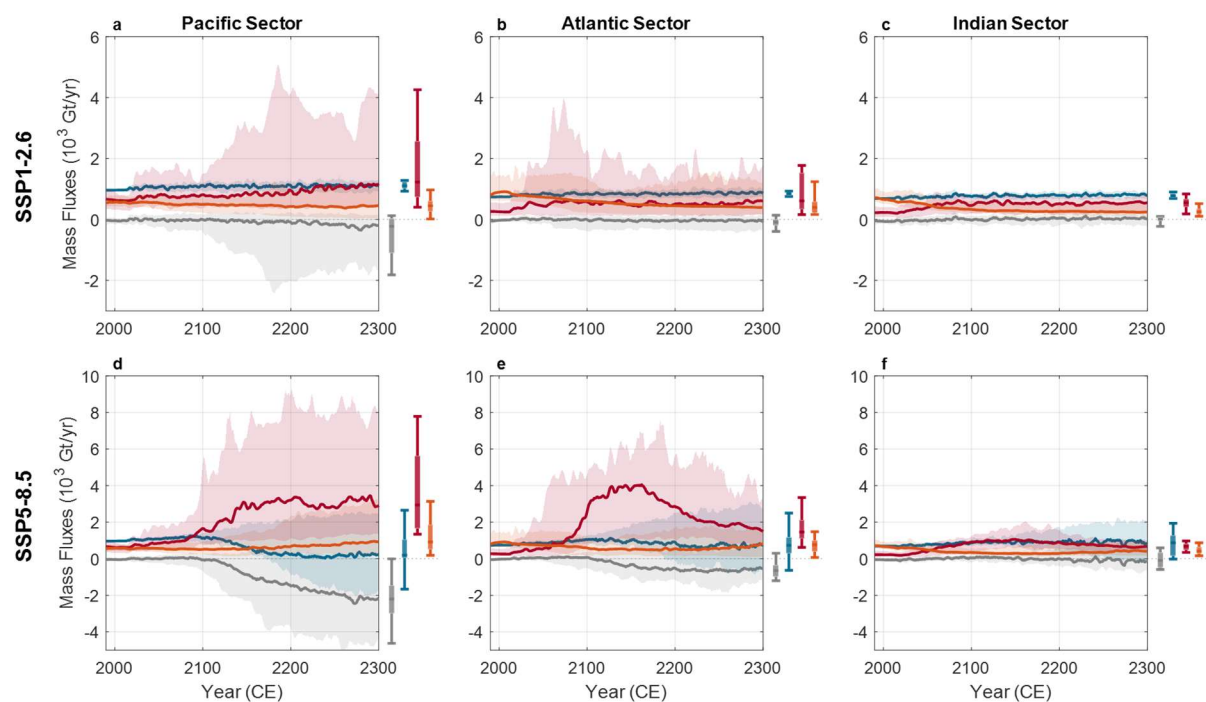


**Fig.8:** Calibrated probabilistic projections of the Antarctic ice sheet mass balance components until 2300 under SSP1-2.6 (a–c) and SSP5-8.5 (d–f) for each ocean sector of Antarctica. Solid lines and shaded regions show the median and 5-95% probability intervals ( $N=100$ ), with a 5-year running average applied. Boxes and whiskers show [5;25;50;75;95] percentiles for the year 2300. Positive SMB fluxes represent mass gains while positive sub-shelf melt and calving fluxes represent mass losses. Note that the ice-sheet net mass balance does not represent the sum of all mass balance components but instead considers changes in volume above flotation and may therefore be interpreted as the rate of mass change contributing to sea-level rise.

#### 4. References

- Adusumilli, S., Fricker, H.A., Medley, B. et al. Interannual variations in meltwater input to the Southern Ocean from Antarctic ice shelves. *Nat. Geosci.* 13, 616–620 (2020). <https://doi.org/10.1038/s41561-020-0616-z>
- BERNALES J, ROGOZHINA I, THOMAS M. Melting and freezing under Antarctic ice shelves from a combination of ice-sheet modelling and observations. *Journal of Glaciology*. 2017;63(240):731-744. doi:10.1017/jog.2017.42
- Bondzio, J. H., Seroussi, H., Morlighem, M., Kleiner, T., Rückamp, M., Humbert, A., and Larour, E. Y.: Modelling calving front dynamics using a level-set method: application to Jakobshavn Isbræ, West Greenland, *The Cryosphere*, 10, 497–510, <https://doi.org/10.5194/tc-10-497-2016>, 2016.
- Bueler, E., and J. Brown (2009), Shallow shelf approximation as a “sliding law” in a thermomechanically coupled ice sheet model, *J. Geophys. Res.*, 114, F03008, doi:[10.1029/2008JF001179](https://doi.org/10.1029/2008JF001179).
- Coulon, V., Klose, A. K., Kittel, C., Edwards, T., Turner, F., Winkelmann, R., and Pattyn, F.: Disentangling the drivers of future Antarctic ice loss with a historically calibrated ice-sheet model, *The Cryosphere*, 18, 653–681, <https://doi.org/10.5194/tc-18-653-2024>, 2024.

Coulon, V., Jan De Rydt, Thomas Gregov, et al. Future freshwater fluxes from the Antarctic ice sheet. ESS Open Archive. July 19, 2024.

DOI: 10.22541/essoar.172135861.19524512/v1

Davison Benjamin J. et al. Annual mass budget of Antarctic ice shelves from 1997 to 2021. *Sci. Adv.* 9, eadi0186 (2023). DOI: [10.1126/sciadv.adi0186](https://doi.org/10.1126/sciadv.adi0186)

DeConto, R., Pollard, D. Contribution of Antarctica to past and future sea-level rise. *Nature* 531, 591–597 (2016). <https://doi.org/10.1038/nature17145>

DeConto, R.M., Pollard, D., Alley, R.B. et al. The Paris Climate Agreement and future sea-level rise from Antarctica. *Nature* 593, 83–89 (2021). <https://doi.org/10.1038/s41586-021-03427-0>

Favier, L., Jourdain, N. C., Jenkins, A., Merino, N., Durand, G., Gagliardini, O., Gillet-Chaulet, F., and Mathiot, P.: Assessment of sub-shelf melting parameterisations using the ocean–ice–sheet coupled model NEMO(v3.6)–Elmer/Ice(v8.3), *Geosci. Model Dev.*, 12, 2255–2283, <https://doi.org/10.5194/gmd-12-2255-2019>, 2019.

Jourdain, N. C., Asay-Davis, X., Hattermann, T., Straneo, F., Seroussi, H., Little, C. M., and Nowicki, S.: A protocol for calculating basal melt rates in the ISMIP6 Antarctic ice sheet projections, *The Cryosphere*, 14, 3111–3134, <https://doi.org/10.5194/tc-14-3111-2020>, 2020.

Kazmierczak, E., Gregov, T., Coulon, V., and Pattyn, F.: A fast and unified subglacial hydrological model applied to Thwaites Glacier, Antarctica, *EGU sphere* [preprint], <https://doi.org/10.5194/egusphere-2024-466>, 2024.shelves

Kittel, C., Amory, C., Agosta, C., Jourdain, N. C., Hofer, S., Delhasse, A., Doutreloup, S., Huot, P.-V., Lang, C., Fichet, T., and Fettweis, X.: Diverging future surface mass balance between the Antarctic ice shelves and grounded ice sheet, *The Cryosphere*, 15, 1215–1236, <https://doi.org/10.5194/tc-15-1215-2021>, 2021.

Lazeroms, W. M. J., A. Jenkins, S. W. Rienstra, and R. S. W. van de Wal, 2019: An Analytical Derivation of Ice-Shelf Basal Melt Based on the Dynamics of Meltwater Plumes. *J. Phys. Oceanogr.*, 49, 917–939, <https://doi.org/10.1175/JPO-D-18-0131.1>.

Morlighem, M., Rignot, E., Binder, T. et al. Deep glacial troughs and stabilizing ridges unveiled beneath the margins of the Antarctic ice sheet. *Nat. Geosci.* 13, 132–137 (2020). <https://doi.org/10.1038/s41561-019-0510-8>

Nias, I. J., Cornford, S. L., Edwards, T. L., Gourmelen, N., & Payne, A. J. (2019). Assessing uncertainty in the dynamical ice response to ocean warming in the Amundsen Sea Embayment, West Antarctica. *Geophysical Research Letters*, 46, <https://doi.org/10.1029/2019GL084941>

Otosaka, I. N., Shepherd, A., Ivins, E. R., Schlegel, N.-J., Amory, C., van den Broeke, M. R., Horwath, M., Joughin, I., King, M. D., Krinner, G., Nowicki, S., Payne, A. J., Rignot, E., Scambos, T., Simon, K. M., Smith, B. E., Sørensen, L. S., Velicogna, I., Whitehouse, P. L., A. G., Agosta, C., Ahlstrøm, A. P., Blazquez, A., Colgan, W., Engdahl, M. E., Fettweis, X., Forsberg, R., Gallée, H., Gardner, A., Gilbert, L., Gourmelen, N., Groh, A., Gunter, B. C., Harig, C., Helm, V., Khan, S. A., Kittel, C., Konrad, H., Langen, P. L., Lecavalier, B. S., Liang, C.-C., Loomis, B. D., McMillan, M., Melini, D., Mernild, S. H., Mottram, R., Mouginot, J., Nilsson, J., Noël, B., Pattle, M. E., Peltier, W. R., Pie, N., Roca, M., Sasgen, I., Save, H. V., Seo, K.-W., Scheuchl, B., Schrama, E. J. O., Schröder, L., Simonsen, S. B., Slater, T., Spada, G., Sutterley, T. C., Vishwakarma, B. D., van Wessem, J. M., Wiese, D., van der Wal, W., and Wouters, B.: Mass balance of the Greenland and Antarctic ice sheets from 1992 to 2020, *Earth Syst. Sci. Data*, 15, 1597–1616, <https://doi.org/10.5194/essd-15-1597-2023>, 2023.

Pattyn, F.: Sea-level response to melting of Antarctic ice shelves on multi-centennial timescales with the fast Elementary Thermomechanical Ice Sheet model (f.ETISh v1.0), *The Cryosphere*, 11, 1851–1878, <https://doi.org/10.5194/tc-11-1851-2017>, 2017.

Pollard, D. and DeConto, R. M.: Description of a hybrid ice sheet-shelf model, and application to Antarctica, *Geosci. Model Dev.*, 5, 1273–1295, <https://doi.org/10.5194/gmd-5-1273-2012>, 2012.

Pollard, D. and DeConto, R. M.: A simple inverse method for the distribution of basal sliding coefficients under ice sheets, applied to Antarctica, *The Cryosphere*, 6, 953–971, <https://doi.org/10.5194/tc-6-953-2012>, 2012.

Pollard, D. and DeConto, R. M.: Improvements in one-dimensional grounding-line parameterizations in an ice-sheet model with lateral variations (PSUICE3D v2.1), *Geosci. Model Dev.*, 13, 6481–6500, <https://doi.org/10.5194/gmd-13-6481-2020>, 2020.

Pollard D., Robert M. DeConto, Richard B. Alley, Potential Antarctic Ice Sheet retreat driven by hydrofracturing and ice cliff failure, *Earth and Planetary Science Letters*, Volume 412, 2015, Pages 112–121, ISSN 0012-821X, <https://doi.org/10.1016/j.epsl.2014.12.035>

Reese, R., Albrecht, T., Mengel, M., Asay-Davis, X., and Winkelmann, R.: Antarctic sub-shelf melt rates via PICO, *The Cryosphere*, 12, 1969–1985, <https://doi.org/10.5194/tc-12-1969-2018>, 2018.

Rignot E. et al, Four decades of Antarctic Ice Sheet mass balance from 1979–2017, *Environmental Sciences*, January 14, 2019, 116 (4) 1095–1103, <https://doi.org/10.1073/pnas.1812883116>

Ritz, C., Edwards, T., Durand, G. et al. Potential sea-level rise from Antarctic ice-sheet instability constrained by observations. *Nature* 528, 115–118 (2015). <https://doi.org/10.1038/nature16147>

Schoof, C. (2007), Ice sheet grounding line dynamics: Steady states, stability, and hysteresis, *J. Geophys. Res.*, 112, F03S28, doi:10.1029/2006JF000664

Smith Ben et al., Pervasive ice sheet mass loss reflects competing ocean and atmosphere processes. *Science* 368, 1239–1242 (2020). DOI: [10.1126/science.aaz5845](https://doi.org/10.1126/science.aaz5845) Sun, S., Cornford, S. L., Moore, J. C., Gladstone, R., and Zhao, L.: Ice shelf fracture parameterization in an ice sheet model, *The Cryosphere*, 11, 2543–2554, <https://doi.org/10.5194/tc-11-2543-2017>, 2017.

van Wessem, J. M., van de Berg, W. J., Noël, B. P. Y., van Meijgaard, E., Amory, C., Birnbaum, G., Jakobs, C. L., Krüger, K., Lenaerts, J. T. M., Lhermitte, S., Ligtenberg, S. R. M., Medley, B., Reijmer, C. H., van Tricht, K., Trusel, L. D., van Ulf, L. H., Wouters, B., Wuite, J., and van den Broeke, M. R.: Modelling the climate and surface mass balance of polar ice sheets using RACMO2 – Part 2: Antarctica (1979–2016), *The Cryosphere*, 12, 1479–1498, <https://doi.org/10.5194/tc-12-1479-2018>, 2018.

Werneck, A., Edwards, T. L., Nias, I. J., Holden, P. B., and Edwards, N. R.: Spatial probabilistic calibration of a high-resolution Amundsen Sea Embayment ice sheet model with satellite altimeter data, *The Cryosphere*, 14, 1459–1474, <https://doi.org/10.5194/tc-14-1459-2020>, 2020.

Wilner, J. A., Morlighem, M., and Cheng, G.: Evaluation of four calving laws for Antarctic ice shelves, *The Cryosphere*, 17, 4889–4901, <https://doi.org/10.5194/tc-17-4889-2023>, 2023.

Winkelmann, R., Martin, M. A., Haseloff, M., Albrecht, T., Bueler, E., Khroulev, C., and Levermann, A.: The Potsdam Parallel Ice Sheet Model (PISM-PIK) – Part 1: Model description, *The Cryosphere*, 5, 715–726, <https://doi.org/10.5194/tc-5-715-2011>, 2011.

## 5. Impact

This deliverable contributes to the following objectives stated in the description of the action.

### **O2: Improve critical ice sheet-ocean processes in numerical models.**

We have included novel processes and interactions previously lacking in ice sheet models, such as ice shelf damage and improved ice shelf calving. We also included a thorough uncertainty analysis of those critical processes.

### **O3: Improve representation of AIS dynamics and integrate this knowledge into ice sheet-climate models.**

We developed and implemented new representations of ice sheet dynamics, such as damage and calving, in the ice sheet model that was used to produce the freshwater fluxes.

### **O4: Quantify AIS melt sensitivity to climate forcing and reduce the ‘deep uncertainty’ in freshwater flux and SLR projections to 2300.**

We have quantified AIS freshwater fluxes and their uncertainty thereby including AIS melt sensitivity by using different subshelf melt and calving models and a large parameter space. Uncertainties are reduced by comparing the model results over the past decades with a series of estimates of regional net mass balance from the latest Ice Sheet Mass Balance Inter-comparison Exercise. Calibrated simulations are then qualitatively assessed with a series of spatially aggregated estimates of ice-sheet net mass balance, surface mass balance, sub-shelf melting, and iceberg calving fluxes from recent satellite- and modelling-based studies.

### **O5: Assess how global ocean circulation is impacted by freshwater discharge from the northern and southern ice sheets.**

The produced AIS freshwater fluxes will be used in WP5 to assess ice sheets impacts on global ocean circulation. Results contribute to improved knowledge of glaciological physical processes and hence improved projections of future SLR by better quantifying uncertainties in AIS projections.

### **O6: Assess the ocean impact on key global climate metrics from polar ice sheet melt to 2300 and beyond.**

The produced AIS freshwater fluxes will be used in WP6 to assess the role of Antarctica in the global climate.

### **O7: Deliver free and open data access and contribute to international assessments, climate model development, observing initiatives and policymakers.**

Our datasets are freely available and will be intensively used by project partners in assessing the impact of distributed freshwater fluxes on global ocean circulation.

## Annex 1: Supplement Table S1: Parameters governing glaciological processes

This table lists the parameters shown in Fig. 2.

**Table S1.** Parameters governing glaciological processes along with their uncertainty ranges used in the uncertainty analysis. The parameters which control the effective ice–ocean heat flux relate to the considered sub-shelf melt parameterisation. The parameter  $\Gamma_{\text{eff}}$  originally takes a value within the range of  $[0 - 1]$ , as defined by the Latin hypercube sampling. It is then applied to the uncertainty range of the parameter associated with  $M_{\text{param}}$ . For instance, for the  $j$ -th simulation of the ensemble, if  $M_{\text{param}}^j$  is the local quadratic parameterisation  $M_{\text{quad}}$ , a  $\Gamma_{\text{eff}}^j$  of 0.5 would correspond to a  $\gamma_T$  of  $5.5 \times 10^{-4} \text{ m s}^{-1}$ . Similarly, the calving parameters  $C_{\text{par}}$  relate to the considered calving law  $C_{\text{law}}$ .

Parameter	Uncertainty range	Units
Sub-shelf melt parameterisation ( $M_{\text{param}}$ )	PICO model ( $M_{\text{PICO}}$ )	-
	Plume model ( $M_{\text{plume}}$ )	
	Local quadratic parameterisation ( $M_{\text{quad}}$ )	
	ISMIP6 non-local quadratic parameterisation ( $M_{\text{JD20}}$ )	
	ISMIP6 non-local quadratic parameterisation with local slope dependency ( $M_{\text{JD20s}}$ )	
Effective ice-ocean heat flux ( $\Gamma_{\text{eff}}$ )	$\gamma_T^*$ in $M_{\text{PICO}}$ : $[0.1 - 10] \times 10^{-5}$	$\text{m s}^{-1}$
	$C_d^{1/2} \gamma_{TS}$ in $M_{\text{plume}}$ : $[1 - 10] \times 10^{-4}$	-
	$\gamma_T$ in $M_{\text{quad}}$ : $[1 - 10] \times 10^{-4}$	$\text{m s}^{-1}$
	$\gamma_0$ in $M_{\text{JD20}}$ : $[1 - 4] \times 10^4$	$\text{m yr}^{-1}$
	$\gamma_0$ in $M_{\text{JD20s}}$ : $[1 - 4] \times 10^6$	$\text{m yr}^{-1}$
Calving law ( $C_{\text{law}}$ )	Crevasse depth law (CD)	-
	Von Mises law (VM)	
	Minimum thickness law (MT)	
Calving parameter ( $C_{\text{par}}$ )	Critical crevasse ratio in CD: $[0 - 1]$	-
	Tensile stress threshold in VM: $[25 - 1000]$	kPa
	Minimum ice thickness threshold in MT: $[50 - 400]$	m
Exponent in sliding law ( $m$ )	$[1 - 5]$	-
Maximum damage ratio (dam)	$[0 - 0.5]$	-
Spatial resolution ( $\Delta x$ )	8	km
	16	
CMIP6 GCM (GCM)	MRI-ESM2-0	-
	UKESM1-0-LL	
	IPSL-CM6A-LR	
	CESM2-WACCM	
Atmospheric lapse rate ( $\gamma_{\text{atm}}$ )	$[-12 - -5]$	$^{\circ}\text{C km}^{-1}$
Degree-day factor for the melting of snow ( $K_{\text{snow}}$ )	$[0 - 6]$	w.e. $\text{mm PDD}^{-1}$
Degree-day factor for the melting of ice ( $K_{\text{ice}}$ )	$[4 - 16]$	w.e. $\text{mm PDD}^{-1}$
Thickness of the thermally-active layer ( $d_{\text{ice}}$ )	$[0 - 15]$	m